

# Circular dichroism of some high-symmetry chiral molecules: B3LYP and SAOP calculations

Carl Trindle · Zikri Altun

Received: 16 July 2008 / Accepted: 19 November 2008 / Published online: 9 December 2008  
© Springer-Verlag 2008

**Abstract** Computational modeling of optical activity, circular dichroism (CD) and optical rotatory dispersion, is rapidly becoming a useful supplement to experimental studies of absolute configuration. Here, we investigate the predictions of two alternative formulations of the rotational strength based on time-dependent density functional theory (TD-DFT), for a series of high symmetry chiral systems. We employ the TD-DFT method as realized in Gaussian 03 suite with the hybrid functional B3LYP and as incorporated in the Amsterdam density functional (ADF) suite with PBE and SAOP functionals. The high-symmetry systems described here are somewhat larger than those used to evaluate the influence of basis sets and density functional choice, and for such large systems the very extensive basis sets recommended by most investigators may not be suitable for routine use. We observe that useful results for these systems can be obtained in modest bases, and in particular that diffuse functions may not be required for informative use of the ADF implementation. The statistical average of orbital potentials (SAOP) model developed by Baerends is essential to the success of the ADF implementation. In some cases chirality is defined by features of the molecular structure remote from the chromophore. This is a severe test of the TD-DFT theory, since

high-lying excitations define the most prominent features of the CD spectra, and complicates the use of computations to guide the assignment of absolute configuration. Experimental investigation of the high symmetry systems described here is desirable.

## 1 Introduction

The computation of circular dichroism (CD) and optical rotatory dispersion (ORD) has been a continuing challenge to chemical theory since the pioneering work of Eyring [1], Moscovitz [2], and Tinoco [3]. Polavarapu [4] reviewed the general terrain of ORD experiment and theory, addressing both empirical models and computational advances to 2002. Crawford [5] has also surveyed the substantial progress which has taken place since the landmark work and review of Hansen and Bouman [6]. The emphasis in recent work has rested on ORD, as shown in reviews by Autschbach [7] and Polavarapu [8]. The advances have been both formal—the formulation of optical properties within linear response theory—and practical, as versions of time-dependent density functional theory models have been incorporated into widely available electronic structure codes. The methods have become so powerful to be useful in the determination of absolute configuration [9].

Optical excitation energies and the rotational strength  $R$  define both ORD and CD.

$$R_{0k} = \text{Im}\langle 0|\boldsymbol{\mu}|k\rangle \cdot \langle k|\mathbf{m}|0\rangle$$

Here  $\mathbf{m}$  is the magnetic dipole moment operator and  $\boldsymbol{\mu}$  is the electric dipole moment operator, both of which mix the ground state 0 and an excited state  $k$ .

**Electronic supplementary material** The online version of this article (doi:10.1007/s00214-008-0494-8) contains supplementary material, which is available to authorized users.

C. Trindle (✉)  
Chemistry Department, The University of Virginia,  
Charlottesville, VA 22904, USA  
e-mail: cot@virginia.edu

Z. Altun  
Physics Department, Marmara University, Istanbul, Turkey

ORD is the result of contributions from many excitations. The magnetic–electric dipole polarizability is defined as

$$\begin{aligned}\bar{\beta}(\omega) &= \frac{2c}{3} \text{Im} \left[ \sum_{k \neq 0} \frac{\langle 0 | \boldsymbol{\mu} | k \rangle \cdot \langle k | \mathbf{m} | 0 \rangle}{\omega_{k0}^2 - \omega^2} \right] \\ &= \frac{2c}{3} \sum_{k \neq 0} \left[ \frac{R_{0k}}{\omega_{k0}^2 - \omega^2} \right]\end{aligned}$$

Here  $\omega_{k0}$  is the frequency corresponding to the transition energy. In computational work atomic units are employed  $\hbar = 1$ ,  $m_e = 1$ ,  $4\pi\epsilon_0 = 1$ ,  $c \approx 137$

The experimentally reported quantity is the specific angle of rotation at the frequency of the incident light.

$$[\alpha]_D = \frac{28,800\pi^2 N_A \omega^2}{4\pi^2 c^2 M} \bar{\beta}(\omega)$$

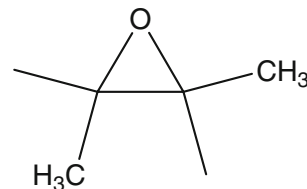
Here  $N_A$  is Avogadro's number,  $M$  the molar mass of the chiral species,  $\omega$  the frequency of the incident radiation, and  $c$  the speed of light. Many measurements use the Na "D" line at 589 nm as the incident light.

Successful modeling of ORD—especially the specific rotation angle which is most usually available from experimental measurement—requires a reasonably accurate representation of the global response of the chiral system to polarized light. Stephens et al. [10] defined a set of test cases for which sodium D-line rotations are known, and observed that density functional (DFT) methods—specifically, B3LYP—perform better than SCF methods. Within B3LYP, a very large basis improved the mean absolute deviation (MAD) between computed and measured values to less than 20° (Supplementary material, Table S1).

Similar performance is found for ADF description of the same test set of molecules [11] (Supplementary material, Table S2). These calculations employed pure density functionals rather than the hybrid B3LYP. The gradient-corrected BP86 functional seems only a bit better than a gradient-free local density approximation (LDA) functional defined by Vosko et al. [12]. SAOP [13], a model for which the long-range behavior of the exchange–correlation energy density functional is defined by a “statistical average of orbital potentials,” seems to improve results modestly. The two large basis sets  $V_p$  (extensively polarized) and  $V_d$  (thoroughly augmented with diffuse functions) [11] seem quite similar in performance. Since the quality of  $V_p$  results is at least comparable to  $V_d$  results, we infer (gingerly) that a high level of polarization is as effective as adding diffuse functions.

Since the ORD is computationally so demanding, we may be better advised first to study the circular dichroism spectra for some well-understood systems. This allows us

to focus on the lowest few excitation energies and associated rotational strengths. Using the CD modules in Gaussian 03 [14] and the Amsterdam density functional [15] software suites we have re-investigated some very well studied systems, including the thoroughly studied dimethyloxirane (shown below). The dimethyloxirane has no chromophore, but has a more symmetric  $C_2$  chiral environment. Both B3LYP and SAOP models predict CD spectra (Supplementary materials, Tables S3, S4) in general agreement with other investigators' reports, and fail in similar ways for  $\beta$  pinene and dimethyloxirane.



A simulation of the dimethyl oxirane spectrum will give an impression of the quality of the computations (see Fig. 1). The simulation is based on the computed rotational strengths  $R_{0j}$  (cgs units  $\times 10^{40}$ ) and excitation energies  $E_j$  (eV), as follows:

$$S_{CD} = \sum_j R_{0j} \left( \frac{w}{\pi} \right)^{1/2} \exp \left[ -w(E_j - E)^2 \right]$$

The normalized Gaussian form is chosen for computational ease and flexibility. The width parameter  $w$  is rather arbitrarily chosen as  $50 \text{ eV}^{-2}$  and is identical for every transition modeled. The rotational strength is expressed in Debye–Bohr magneton units, or numerically  $0.9274 \times 10^{-38}$  cgs units ( $\text{erg cm}^3$ ). Computed values of the rotational strength are often reported in multiples of  $10^{-40}$  cgs, and we have chosen this as our common vertical axis. The experimental values of rotational strengths are obtained from measurements of the difference in

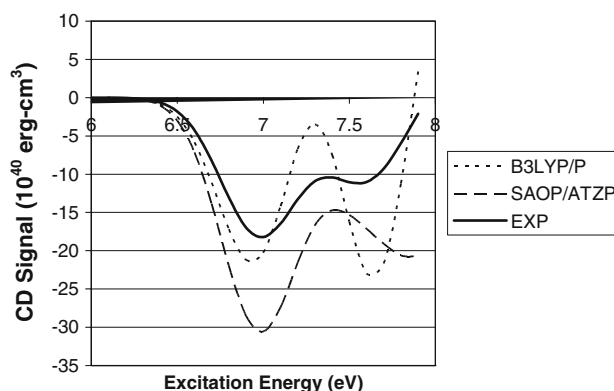


**Fig. 1** Simulated circular dichroism spectrum of dimethyloxirane

absorption coefficients for left and right circularly polarized light,  $\Delta\epsilon$ . According to Fasman [16], one may use the approximation

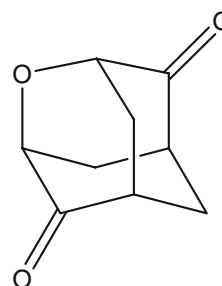
$$R_{\text{exp}}[\text{cgs}] = 2.295 \times 10^{-39} \int \frac{\Delta\epsilon}{\lambda} d\lambda \\ \approx 4.068 \times 10^{-39} \frac{\Delta\epsilon_{\text{max}}}{\lambda_{\text{max}}} h$$

assuming the experimental spectral feature is modeled by a Gaussian centered at  $\lambda_{\text{max}}$ , of height  $\Delta\epsilon_{\text{max}}$  and of width  $h$ . Our simulated spectra resemble smoothed experimental spectra (no vibrational structure is incorporated), and represent the theoretical and experimental estimates of rotational strengths faithfully and equivalently.

The solid line, intended to represent experimental data, is constructed with the rotational strengths and excitation energies deduced by Breest et al. [17] This analytical representation washes out much of the structure of the experimentally recorded CD spectrum. However, it permits a visual comparison between equivalently derived representations of the spectrum. For the simulated spectra derived from computations, we use the first nine excitations and associated rotational strengths; usually only a few such parameters are available from experimental work. All calculations of the dimethyloxirane reveal the strong negative leading feature, show a weak second feature with positive sign, and capture the sign alternation associated with the next two transitions. By comparison with the SAOP model, the B3LYP functional displays a red shift and an exaggerated positive feature in the lower energy reaches of the spectrum. However, it is evident that the high energy reaches of the CD spectrum are not realistically represented even by the SAOP/ATZP model. We should note that these calculations, which describe only electronic contributions to the rotational strengths and circular dichroism spectra, overlook vibronic effects critical to the accurate depiction of optical activity of this molecule [18]. Crawford et al. [19] point out a number of cases for which electronic structure calculations of CD are still problematic.

We have now established a level of expectation for the semi-quantitative performance of the Gaussian and ADF TD-DFT description of optical excitation energies and rotational strengths. It seems that at the very least, we can rely on the computed sign of the lowest energy signal and in most cases also trust the sign of the next feature. Although high-energy reaches of the spectrum are not generally represented well, this limited success is sufficient to make calculations a useful adjunct to (or even corrective to) empirical generalization such as the octant rule. For example, Žilinskas et al. [20] have established the absolute configuration of the  $C_2$ -symmetric (+)-2-oxadamantane-4,8-dione with the help of the octant rule [21] for the  $n - \pi^*$

transition of the C=O groups, which they employed to interpret the CD spectrum. In that spectrum they observe a positive feature at about 310 nm (ca 4.0 eV), and the beginning of a negative feature at wavelengths shorter than about 240 nm (ca 5.2 eV). Our B3LYP calculations (Supplementary material, Table S5) put the positive feature slightly to the red at 3.95 eV and the more intense negative feature 1.0 eV higher, at 4.95 eV. The calculation supports the assignment based on the octant rule.



The SAOP/ATZP calculation shifts the leading edge further to the red (to 3.7 eV), and seems to compress the sequence of excited states. The stronger negative feature lies only about 0.5 eV above the lowest energy band. Despite this significant compression, the general form of the SAOP/ATZP spectrum resembles the B3LYP/6-311++G(2d,2p) form, as shown in Fig. 2. The SAOP energies have been shifted by 0.4 eV so to emphasize the similarity in general form.

Since the implementation of the TD-DFT algorithm for CD modeling in B3LYP has proved its practical value by assisting the assignment of absolute configurations [22], it will be important to see if alternative methods provide consistent descriptions of the major features of the CD spectrum for representative systems. We choose to study a variety of systems with  $D_2$  symmetry.

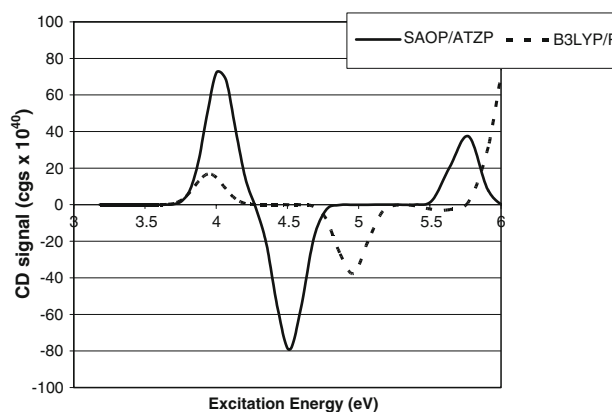


Fig. 2 Simulated spectra of 2-oxadamantane-4,8-dione

## 2 Circular dichroism of high symmetry molecules

High symmetry molecules have enduring appeal to synthesists and theoretical analysts owing to their beauty and simplicity: examples of highly sought synthetic targets include cubane, propellanes, icosahedranes and even the highly strained tetrahedrane [23]. An especially interesting set of high symmetry molecules also display chirality, owing to the absence of a plane of symmetry.  $C_2$ - and  $C_3$ -symmetric chiral molecules are of special interest in catalysis [24, 25] for practical reasons beyond their aesthetic appeal. Farina and Morandi [26] reviewed the collection of such molecules known in the 1970s, which achieved  $C_2$ ,  $C_3$ ,  $D_2$ , and  $D_3$  symmetry. Nakazaki [27] extended the set, constructing systems with symmetry as high as  $T_d$ . New symmetric chiral systems are regularly reported [28, 29].

Following up the hint that modest basis sets may be effective in modeling CD and ORD in medium to large systems, we present a series of computations which embrace relatively large molecules, with high symmetry so that calculations with flexible basis sets are within reach. We first choose  $D_2$  systems with familiar chromophores including monoalkenes, carbonyls, and twisted and stacked phenyls.

### 2.1 Species A: a chiral saturated diether

The diether A shown below, structure number 25b in Farina-Morandi [26], is a distant echo of the oxirane system, and tests our hope that a modest basis can perform well for medium-sized molecules in which—there being no chromophore—transitions are likely to have considerable Rydberg character. The chirality stems from the skewed dimethylene bridges, so we do not expect large values of rotational strengths.

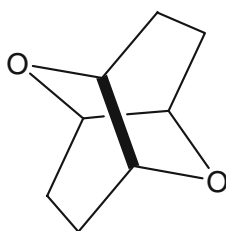


Figure 3 displays excitation energies computed for each state in eight models. Within each cluster labeled by an electronic excitation we find the B3LYP models at left; in order from left: B3LYP/S//B3LYP/S, B3LYP/L//B3LYP/S, and B3LYP/P//B3LYP/S. Here  $S$  = “Small” or 6-31G( $d$ );  $L$  = “Large” or 6-311+ G( $d,p$ ); and  $P$  = “Preferred” or the recommended basis set 6-311 ++G(2 $d,2p$ ). There is a

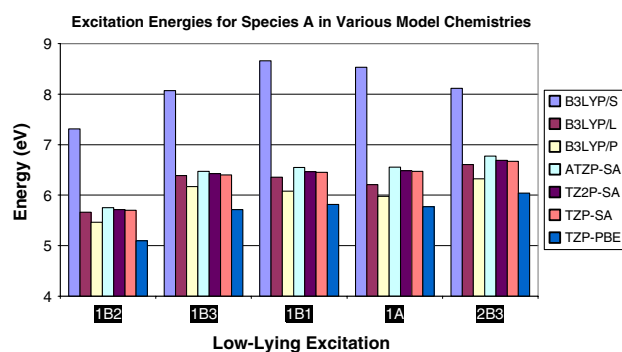


Fig. 3 Excitational energies for the chiral diether A

substantial lowering of excitation energy as we pass from  $S$  to  $L$ , but a lesser change as we continue from  $L$  to  $P$ . At far right is the energy predicted by PBE/TZP//PBE/DZP. Continuing right to left, we find results for SAOP/TZP//PBE/DZP; SAOP/TZ2P//PBE/DZP; and SAOP/ATZP//PBE/DZP. Only the ATZP basis includes diffuse functions. Numerical values are to be found in Supplemental material, Table S6. SA refers to the SAOP functional. ATZP = triple zeta with polarization, augmented with diffuse functions.

Within any cluster of estimates of the energy of a specific excitation, we see that the value at far left, referring to B3LYP/6-31G( $d$ ), is persistently high, but the value of the B3LYP excitation energy stabilizes as the basis is improved. Even the lowest energy excitations are sensitive to the presence of diffuse functions. PBE/TZP excitation energy values at far right in any cluster are small (very red). The pronounced blue shift from TZP-PBE to TZP-SAOP suggests that even the lowest energy transition to the red of 6 eV has substantial Rydberg character. Use of the SAOP functional produces stable estimates already for the TZP basis, little changed for bigger basis sets.

The sequence of excitations in Fig. 3 is taken from SAOP/ATZP excitation values. There is disagreement in the sequence of excitations between SAOP/ATZP and B3LYP/P. In the former case, the first  $B_3$  excitation is estimated to lie at higher energy than the first  $B_1$  and  $A$  excitations; in either model these levels all lie within a narrow (0.2 eV) band.

Figure 4 shows rotational strengths for each of the low-lying excitations, for the same collection of model chemistries.

Figure 4 shows the dependence of computed rotational strengths on model chemistry for species B. Models include basis  $S$  = 6-31G( $d$ ),  $L$  = 6-311+G( $d,p$ ) and  $L$  = 6-311++G(2 $d,2p$ ). SA refers to the SAOP functional. ATZP = triple zeta with polarization, augmented with diffuse functions.

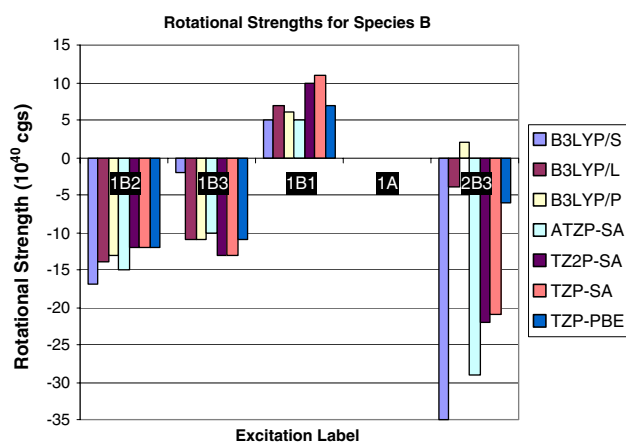


**Fig. 4** Rotational strengths for low-energy excitations for diether B

The magnitude of species B's rotational strengths is modest, as expected. Calculations in B3LYP and SAOP agree that the first features of the CD spectrum should be negative, followed by a positive signal. Diffuse functions in SAOP/ATZP have a noticeable effect on rotational strength even for these low-energy transitions. SAOP provides a sign-consistent treatment of the higher-energy  $2B_3$  excitation's rotational strength, while B3LYP results for the  $2B_3$  excitation vary considerably with basis. B3LYP/Small predictions seem to get signs right, as do those from PBE/TZP.

Figure 5 shows that the simulated spectra are very consistent. One would be confident that these calculations of the CD spectrum would be useful for experimental assignment of configuration.

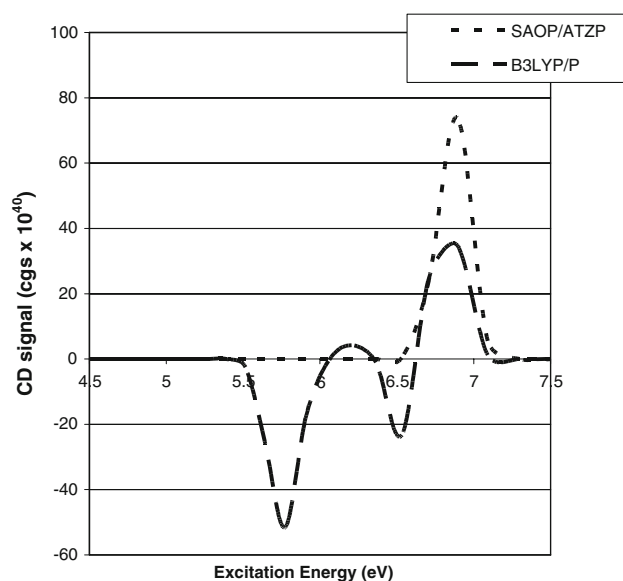
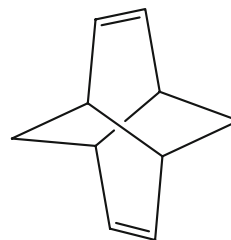


**Fig. 5** Simulated spectrum for chiral ether A

## 2.2 Species B: skewed CC double bonds

The motif of twisted double bonds is a venerable model in optical activity calculations, serving as the smallest chiral system of high symmetry and (in the form of  $C_2$ -symmetric *trans*-cyclooctene) a test for the most advanced calculations [30]. Species B (structure number 27 in Farina and Morandi's scheme [26] and shown below) is a twisted diene. However, the double bonds of species B, oriented at about  $60^\circ$  to one another, are not seriously deformed; the structure coupling the relatively skewed pi bonds is itself chiral, defining a global  $D_2$  symmetry. This suggests the rotational strength of this system will be small.



The low-energy features of the CD spectrum estimated with TD-DFT, by the B3LYP functional implemented in GAUSSIAN and the SAOP model in ADF are summarized in Fig. 6. (Numerical values may be found in supplemental material, Table S7). These transitions are all dominated by single excitations: for example the  $1B_2$  transition arises primarily from orbital excitation  $9b_2 \rightarrow 11a$  (HO-LU), while the  $1B_1$  transition is almost entirely represented by the orbital excitation  $9b_2 \rightarrow 9b_3$  and  $2B_2$  by  $9b_2 \rightarrow 12a$ . TDDFT seems to be reliable for such transitions.

Figure 6 shows the dependence of computed excitation energies on model chemistry for species B. Abbreviations are as defined for Fig. 3.

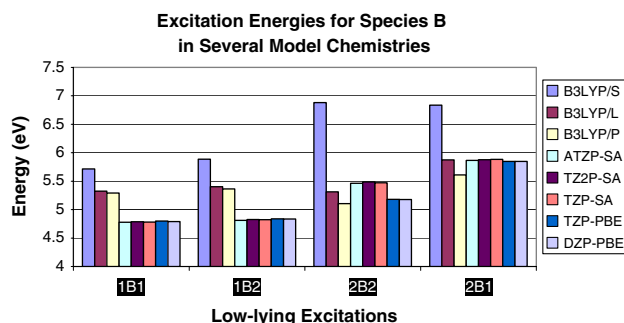


**Fig. 6** Excitation energies for the chiral diene B

The figure displays symmetry-labeled excitation energies computed for each state in eight models, ordered within each excitation's cluster as in the discussion of the diether B. Here we have also included PBE/DZP//PBE/DZP at far right. We observe only a minor change as we pass from DZ to TZP bases with the PBE functional, but note a response to the SAOP device for the  $2B_2$  transition. From this we may infer that this state may have some Rydberg character. Within the group SAOP/TZP//PBE/DZP; SAOP/TZ2P//PBE/DZP; and SAOP/ATZP//PBE/DZP excitation energies are remarkably consistent. In B3LYP the excitation energies are sensitive to the basis chosen; there is a substantial lowering of B3LYP excitation energy as we pass from basis set *S* to basis set *L*, but a lesser change as we continue from *L* to *P* (preferred). Even the sequence of the lowest-lying states is not well established, changing as we pass from *L* to the recommended basis *P*. Excepting the lowest-energy excitations, the SAOP estimates of transition energies are generally higher (bluer) than the hybrid-functional values of excitation energies. The lowest two states are nearly degenerate as described by SAOP, but do not cross as the basis changes.

We have exchanged the order of energy of excitations  $1B_2$  and  $2B_2$  as computed in B3LYP. Our motive was to match the sequence of signs of rotational strengths for the low-lying excitations, as shown in Fig. 7.

Figure 7 shows the rotational strengths for the four lowest energy excitations. Abbreviations are defined as in Fig. 4.

The figure shows that rotational strengths computed in B3LYP are sensitive to choice of basis. In contrast to B3LYP values, estimates of rotational strengths obtained by the SAOP device are also almost independent of basis. Thus we place more trust in the SAOP/ATZP results than the hybrid TD-DFT predictions.

The simulated CD spectra for Species B (Fig. 8) show the impact of the inconsistent treatment of the  $B_2$  excitation energies. For the first two transitions in SAOP/

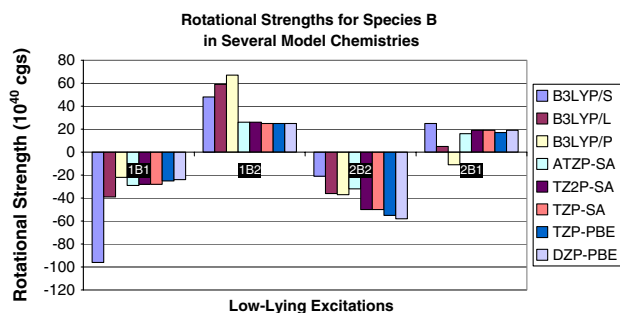


**Fig. 7** Rotational strengths for species B in several model chemistries

ATZP the rotational strengths are large but have opposite signs; the absorption energies are so close that these features tend to cancel. However B3LYP attributes negative rotational strength to both its low-lying levels  $1B_1$  and  $1B_2$ . The  $2B_2$  excitation is attributed a positive rotational strength in B3LYP, so we suspect once again there is a discrepancy in energy ordering. The  $2B_2$  excitation computed in SAOP/ATZP shares the negative sign attributed to  $1B_2$  in B3LYP.

In the discussion of species C–F we will make reference only to the B3LYP/6-311++G(2d,2p) and SAOP/ATZP calculations. Results of model chemistry surveys analogous to those presented for Species A and B are available in the supplementary material, Tables S8, S9, S11 and S12.

### 2.3 Species C: twisted biphenyl linked by propanone bridges

Species C [structure number 23 in Farina-Morandi [26] and shown below, is a member of a family of biphenyls investigated by Mislow [31, 32]. This system combines the chiral biphenyl system with the carbonyl chromophore. Mislow's ORD measurements reveal marked optical activity. The experimental UV spectrum obtained in iso-octane solvent displays a low-intensity feature (from the  $n - \pi^*$  excitation) from 300 to 320 nm or 4.1–3.8 eV; both the B3LYP and SAOP models recapture these  $B_3$  transitions, though the pure DFT errs to the red (3.51 eV, as opposed to B3LYP/P value of 4.04 eV) (see Table S16). The higher energy and more intense ( $\pi - \pi^*$ )  $B_1$  absorptions are observed at 260 (4.8 eV) and 230 nm (5.4 eV).

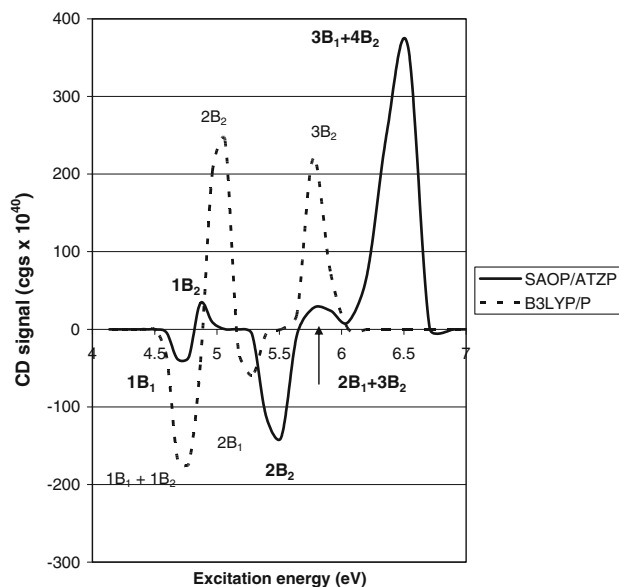
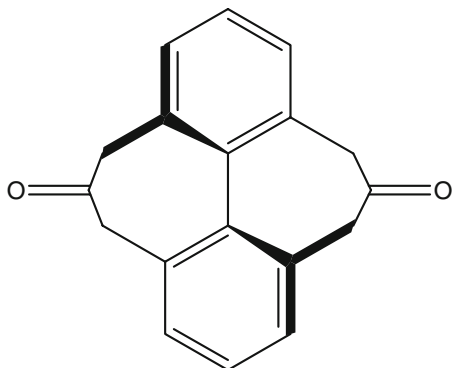


**Fig. 8** Simulated spectrum for chiral diene B

Both TD-DFT methods underestimate these excitation energies: B3LYP in the preferred basis places them at 4.54 and 5.10 eV, while the SAOP model with the ATZP basis places them at 3.91 and 4.29 eV. It seems clear that the quantitative values of pure DFT estimates are not to be trusted in this kind of system.



Predictions of the order of higher energy states by the two methods disagree, with SAOP placing 2A lower than  $2B_3$  (3.96 vs. 4.21 eV) and B3LYP disagreeing (4.86 vs. 4.56 eV). Furthermore, the two models' computed rotational strength for  $2B_3$  disagree drastically: B3LYP predicts -62 with SAOP/ATZP gives +42. We do have confidence in the energy sequence and sign of the rotational strength of first two active transitions ( $1B_3$  and  $1B_1$ ) since that seems invariant across models and basis sets. Perhaps this is sufficiently informative that the calculations can actually assist with the task of interpreting the experimental CD spectrum?

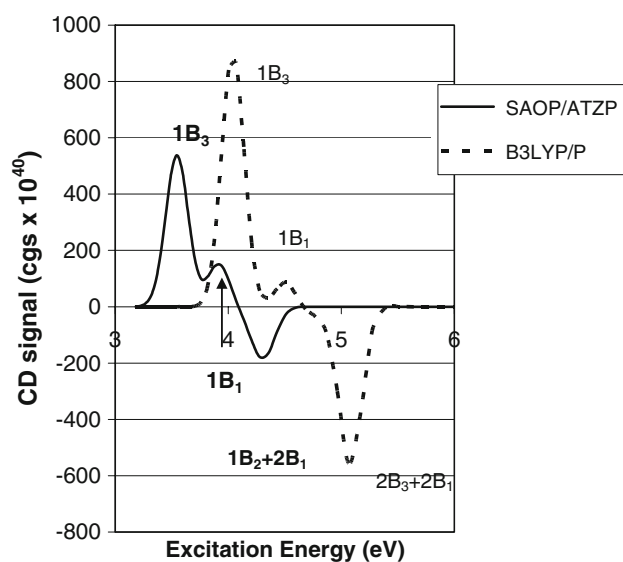
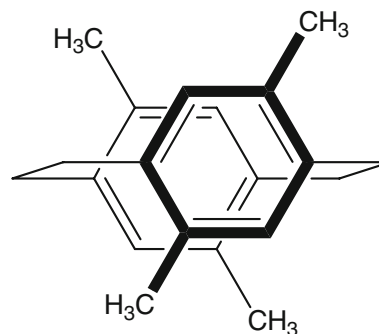


**Fig. 9** Simulated spectrum for biphenyl dione C

The simulated spectrum presents a more encouraging picture of the results; the pronounced reddening of the SAOP model is evident, but the overall forms of the spectra predicted in the two models are remarkably similar for the low-energy region of the spectrum (Fig. 9).

#### 2.4 Species D: twisted xylenes

Species D (structure number 30 in Farina-Morandi [26] and shown below) consists of two xylenes, connected by para  $C_2H_4$  links and twisted by  $60^\circ$  to achieve chirality and  $D_2$  symmetry. The chirality derives from methyl substitution of the stacked-phenyl chromophore, so the rotational strengths are likely to be small except for the transitions with serious Rydberg or methyl CH sigma antibonding character. These transitions involve excited states which are so far extended in space that they will embrace the chiral region.



As shown in Table S17, hybrid-density B3LYP based estimates of the excitation energies are not sensitive to basis set in this case. Results from the preferred basis recommended by Stephens et al. [10, 22] seem very closely comparable to those of the large basis, which suggest the basis effects have been captured already in the more modest basis. Similarly further augmentation seems to have only modest effects on the ADF TZP-SAOP outcome.

Once again the excitation energies predicted by the PBE and SAOP density functionals are red-shifted, by almost 0.5 eV(!) relative to the values obtained by B3LYP in Gaussian. The SAOP and B3LYP predictions of the sequence of states are not consistent, but this may be ascribed to the fact that the excitations are very densely spaced beyond the first two transitions. Rotational strengths for the low-energy transitions are quite inconsistent but mostly small. The methods all agree that the leading edge of the CD spectrum will be negative as shown in Fig. 10 and that the next higher-energy feature will be positive. The low energy edge of the computed spectrum derives from the  $3B_2$  and  $3B_3$  excitations according to both SAOP

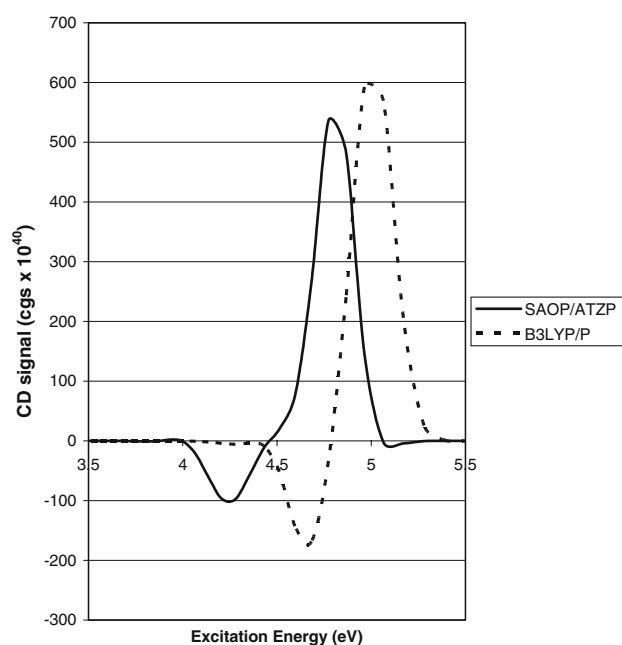


**Fig. 10** Simulated spectra for stacked phenyl D

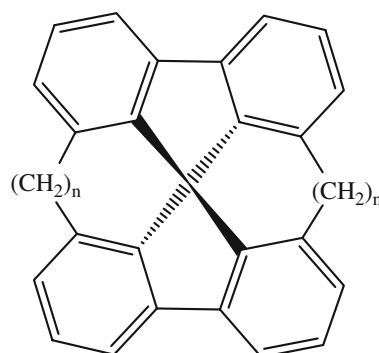
and B3LYP. These have rotational strengths of opposite sign, so the simulated spectrum shows a partial cancellation of the two. The strong positive signal comes from the six  $B_2$  excitation according to the SAOP model,  $4B_2$  in B3LYP.

## 2.5 Vespirene

The vespirenes, a special case of the 9,9'-spirobifluorenes, were studied by Prelog's group [33]. The structure of the  $D_2$ -symmetric species  $[n, n]$ -system with  $n$ -carbon chains is shown. These species are remarkable in that there is a central carbon with four identical substituents, but the overall chirality produces exceptionally large optical activity. The CD spectrum for [6,6] vespirene was analyzed in an exciton model by Haas et al. [33] and separately by Wagniere [34]; Sagir et al. [35] interpreted its CD spectrum by determining Cotton effects for each feature of the optical spectrum.

Extending the linking chains from six to seven or eight carbons weakens the CD and ORD signals only moderately. The experimental UV spectrum has a leading edge absorption at about 320 nm (3.9 eV), another at about 300 nm (4.1 eV), and a broad absorption band peaking at about 270 nm (4.6 eV). In the experimental CD spectrum there is a leading negative feature at about 320 nm, an intervening positive feature at 300–310 nm, a strong negative excursion from 280 to 300 nm (4.3 eV), and a positive signal peaking at 270 nm. The figures depicting

the original experimental spectra from Haas et al. [33] are reproduced in the supplementary material.



The size of this system tested the capability of our equipment, and prohibited use of the preferred basis set for B3LYP. However, the TD-DFT B3LYP model with a 6-311+G( $d,p$ ) basis places the strong low-energy negative signal at 4.0 eV, a positive signal at 4.1 eV, and a collection of excitations with net negative CD over the range 4.25–4.35 eV. All this is entirely—even remarkably—consistent with the experimental spectrum. Even the negative feature at about 230 nm (5.0 eV) has a computed counterpart at 4.6 eV, though we must discount the DFT results at such high energy. The SAOP model in the TZP basis orders states in the same sequence as does B3LYP, and computes  $B_1$  excitations to have negative rotational strength while  $B_3$  excitations have positive rotational strength, but places excitation energies far to the red of the B3LYP estimates.

Simulated CD spectra for 6,6-vespirene are shown in Fig. 11. The red edge of the SAOP/TZP spectrum is located at 3.36 eV. Shifting the SAOP spectrum by 0.45 eV shows the qualitative match between the B3LYP and SAOP traces, which may not be evident from the tabulated excitation energies and rotational strengths.

## 3 Difficult cases

We suspect that systems with chirality deriving from substituents distant from the chromophore will present a considerable challenge to computational modeling. Here we describe our efforts to characterize the CD spectra of two such systems, a dione and an allene.

### 3.1 Species E: a chiral cyclobuta-1,3-dione

Species E (structure number 20 in Farina-Morandi [26] and shown below) is a cyclobuta-1,3-dione system with spiro *trans*-dimethylcyclopentanes defining the  $D_2$

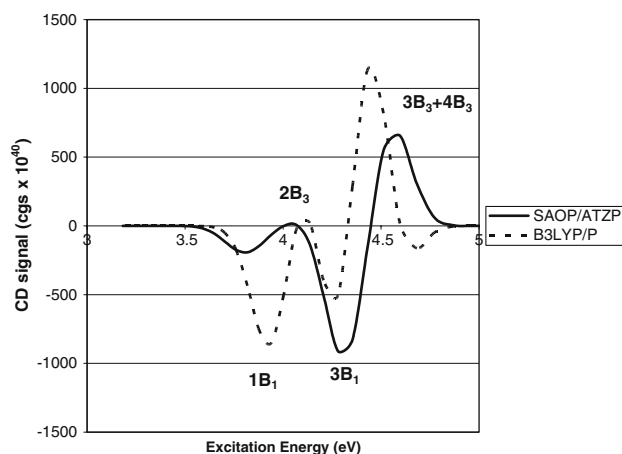
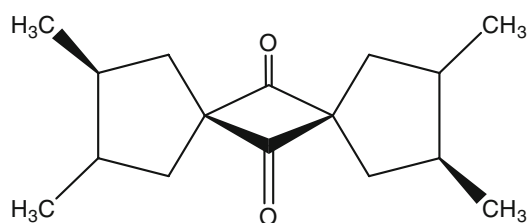


**Fig. 11** Simulated spectra for 6,6-vespirene

symmetry and chirality. (A very similar system with two methyls at the remote carbons has  $S_4$  symmetry and thus is achiral). The optical spectrum will be defined primarily by the carbonyl groups in the central cyclobuta-1,3-dione fragment. The chirality on the other hand is defined by the methyl substitution, which is rather far from the chromophoric carbonyl groups. Consequently, the rotational strengths of low-lying (valence shell) transitions are expected to be small, and the optical activity will be defined by extended and diffuse excited states. We observed that the transitions with significant rotational strength are composed of excitations from the carbonyl chromophore into diffuse orbitals in the neighborhood of the methyl substituents, ( $3B_3$ ) or excitations from the chiral sigma framework into the chromophore's  $\pi^*$  manifold ( $4B_3$ ). This combination of high excitation and charge transfer will be a challenge to the TD-DFT method.



The simulated CD spectra in B3LYP and the SAOP models are shown in Fig. 12. We see that the SAOP excitation energies are far to the red of B3LYP values. The relatively intense feature predicted by SAOP/ATZP as the first  $B_3$  excitation near 5.5 eV is not located by B3LYP until  $4B_3$  at 6.5 eV. According to B3LYP none of the low-lying states from 3.3 to 6.5 eV have significant rotational strengths ( $>10$  units).

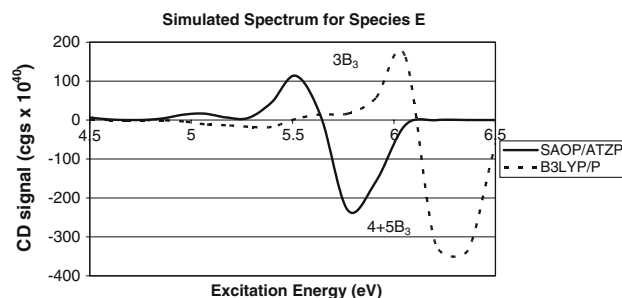
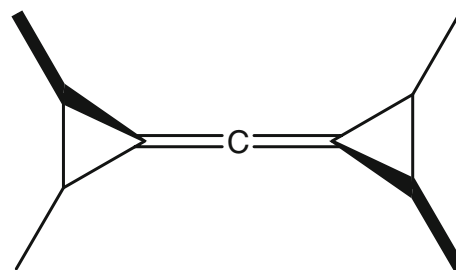


**Fig. 12** Simulated spectra of species E

### 3.2 Species F: a $D_2$ -symmetric allene

Species F (structure number 15 in Farina-Morandi [26] and shown below) is a  $D_2$ -symmetric allene. The electronic structure of the  $D_{2d}$  allene core is itself a considerable challenge to model. The lowest two transitions are agreed to derive from  $e \rightarrow e \pi\pi^*$  transitions of symmetry  $A_2$  and  $B_1$ , followed by a Rydberg transition of symmetry E and the intense  $B_2$  transition (Table 1). The latter excitation is located at 7.1 eV by model chemistry M1 = CASS-CF(8,10)/ANO(++) and near 7.6 by both MRCI+D/ANO(++) and M2 = EOM-CCSD/6-311++G(d,p) [36]. B3LYP/P places this key transition at 7.17 eV, SAOP/TZP at 7.76 eV, and SAOP/ATZP at 7.53 eV. This pattern is maintained for higher transitions as well. As is to be expected, higher excitations have considerable Rydberg character and require diffuse functions even with the SAOP functional.



As was the case for Species E, higher energy transitions are of considerable importance in the CD of Species F, since the peripheral features of the structure which make the molecule chiral are far from the central chromophore. Estimates of the lowest energy excitation in both models cluster in the range 4.8–5.1 eV regardless of basis. In the TD-DFT calculations with the hybrid B3LYP functional, the low-lying states are stable with respect to enhanced basis, while excitations above about 6 eV respond to added polarization and diffuse functions.

The SAOP device shifts the higher energy TZP excitation energies to the blue relative to PBE/TZP, while adding diffuse functions has a modest impact on low-energy

**Table 1** B3LYP and SAOP description of allene optical spectrum

Excitation	Energy (Osc) computed in various models				
	B3LYP/P	M1	M2	SAOP/TZP	SAOP/ATZP
$1^{-1}A_2$	5.775 (0)	6.10	6.23 (0)	5.7329 (0)	5.7264 (0)
$1^{-1}B_1$	5.978 (0)	6.55	6.65	5.9913 (0)	5.9601 (0)
$1^{-1}E$	6.484 (0.0192)	6.94	7.02 (0.030)	7.0791 (0.0184)	6.9606 (0.012)
$2^{-1}A_1$	6.993 (0)		7.69 (0)	8.9879 (0)	8.4282 (0)
$1^{-1}B_2$	7.166 (0.538)	7.56	7.62 (0.411)	7.7610 (0.935)	7.5398 (0.768)
$2^{-1}E$	7.142 (0.0174)		7.82 (0.0172)	7.7798 (0.0359)	7.7024 (0.030)
$2^{-1}B_2$	8.124 (0.234)		8.61 (0.083)	9.3580 (0.170)	8.8017 (0.174)
$3^{-1}E$	8.254 (0.0258)		8.46 (0.019)	9.8434 (0.0230)	8.7502 (0.020)
$4^{-1}E$	9.085 (0.0047)		9.25 (0.0013)		9.0838 (0.021)

excitations but red-shifts the higher energy excitations. This stability of the lowest three excitations to introduction of diffuse basis functions reinforces our idea that these—but not the higher energy excitations—are primarily valence-shell in character.

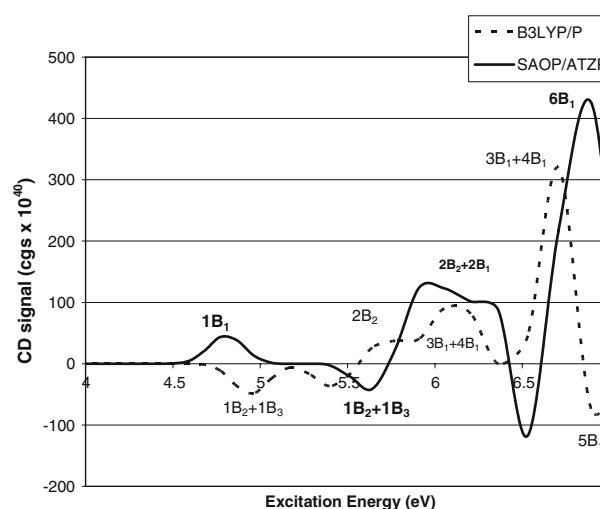
The SAOP/ATZP and B3LYP/preferred estimates of the leading feature of the computed CD spectrum (the  $1B_1$  excitation) disagree in sign. This inconsistency is puzzling; none of the features higher in energy disagree in sign, so long as the basis is TZP or better for SAOP or 6-311+G(*d,p*) or better for B3LYP. The PBE/TZP model produces a spectrum (not shown) very similar to the B3LYP model in the medium and preferred basis sets which are augmented by diffuse functions. The sign reversal seems to be associated with the SAOP model.

The lowest energy transitions—confined as must be to the valence region of the chromophore—cannot dominate the CD spectrum. In this case we had to study about 30 excitations to locate the intense features shown in the simulated spectrum of Fig. 13.

The simulated spectra show some similarity at higher energies; the  $B_2$  and  $B_3$  features are dominated by single excitations. The transition with the greatest rotational strength ( $6B_1$  in both cases) is composed of several one electron excitations, strongly mixed.

#### 4 Conclusions

Choosing highly symmetry chiral species allows computational investigation of CD spectra for large systems with good basis sets. Such study permits conclusions to be drawn on the value of calculations on chiral systems of medium size with basis sets more modest than those recommended in investigations of smaller chiral systems. The lower CD transition energies and associated rotational strengths for systems with familiar chromophores—carbonyl, phenyl, coupled pi bonds—are well described by TD-DFT with a TZP basis without augmentation by diffuse functions so

**Fig. 13** Simulated spectra of species F

long as the statistical average of orbital potentials SAOP functional is used. Even a polycyclic dioxa system (that is, a diether) that would seem to require Rydberg orbitals for reasonable description is consistently represented in this way. TD-DFT with a hybrid density functional theory describes these high-symmetry systems reasonably well within 6-311+G(*d,p*), a smaller basis than is recommended. TD-DFT with pure and hybrid functionals produces qualitatively similar spectra but excitation energies are often significantly energy shifted. In cases for which the structural feature defining chirality is remote from the chromophore, very highly excited states dominate the CD spectra. TD-DFT, which ordinarily can be trusted only for relatively low excitation energies (say half of the ionization energy) performs better than might be predicted. The question remains whether the computationally more difficult but experimentally more easily accessible ORD can be usefully approximated in modest basis sets. In any attempt to assign absolute configuration with computational aid, we recommend study of analog systems, use of several model chemistries, and appropriate caution.

We have reported predictions of CD spectra for a variety of systems which have been made long ago but for which spectra are not yet available. The broad consistency of the results of SAOP and B3LYP predictions encourage us that computational methods will help to guide assignment of spectra and absolute configuration. But the discrepancies among the quantitative details of the methods' predictions point out the need for experimental study. Complementary data from experiment will allow more subtle understanding of the reliability of TD-DFT methods, and a deeper appreciation of the role of solvent media.

**Acknowledgments** Our thanks to the chemistry department, the Parents' Fund and the Office of the Provost of the University of Virginia, the physics department of Marmara University, and the Body Foundation for making this work possible.

## References

- Caldwell DJ, Eyring H (1971) The theory of optical activity. Wiley, New York
- Moscowitz A (1962) Adv Chem Phys 4:67. doi:10.1002/9780470143506.ch2
- Tinoco I (1962) Adv Chem Phys 4:113. doi:10.1002/9780470143506.ch3
- Polavarapu PL (2002) Chirality 14:768. doi:10.1002/chir.10145
- Crawford TD (2006) Theor Chem Acc 115:227. doi:10.1007/s00214-005-0001-4
- Hansen AE, Bouman TD (1980) Adv Chem Phys 44:545. ed Prigogine I, Rice SA, John Wiley and Sons, New York. doi:10.1002/9780470142639.ch5
- Autschbach J (2007) Comput Lett 3:131
- Polavarapu PL (2007) Chem Rec 7:125. doi:10.1002/tcr.20117
- Stephens PJ, McCann DM, Cheeseman JR, Frisch MJ (2005) Chirality 17:S52. doi:10.1002/chir.20109
- Stephens PJ, Devlin FJ, Cheeseman JR, Frisch MJ (2001) J Phys Chem A 105:5356. doi:10.1021/jp0105138
- Autschbach A, Patchkovskii S, Ziegler T, van Gisbergen SJA, Baerends EJ (2002) J Chem Phys 117:581. doi:10.1063/1.1477925
- Vosko SH, Wilk L, Nusair M (1980) Can J Phys 58:1200
- Gritsenko OV, Schipper PRT, Baerends EJ (1999) Chem Phys Lett 302:1999. doi:10.1016/S0009-2614(99)00128-1
- Gaussian 03, Revision C.02, Frisch MJ, Trucks GW, Schlegel HB, Scuseria GE, Robb MA, Cheeseman JR, Montgomery JA Jr, Vreven T, Kudin KN, Burant JC, Millam JM, Iyengar SS, Tomasi J, Barone V, Mennucci B, Cossi M, Scalmani G, Rega N, Petersson GA, Nakatsuji H, Hada M, Ehara M, Toyota K, Fukuda R, Hasegawa J, Ishida M, Nakajima T, Honda Y, Kitao O, Nakai H, Klene M, Li X, Knox JE, Hratchian HP, Cross JB, Bakken V, Adamo C, Jaramillo J, Gomperts R, Stratmann RE, Yazyev O, Austin AJ, Cammi R, Pomelli C, Ochterski JW, Ayala PY, Morokuma K, Voth GA, Salvador P, Dannenberg JJ, Zakrzewski VG, Dapprich S, Daniels AD, Strain MC, Farkas O, Malick DK, Rabuck AD, Raghavachari K, Foresman JB, Ortiz JV, Cui Q, Baboul AG, Clifford S, Cioslowski J, Stefanov BB, Liu G, Liashenko A, Piskorz P, Komaromi I, Martin RL, Fox DJ, Keith T, Al-Laham MA, Peng CY, Nanayakkara A, Challacombe M, Gill PMW, Johnson B, Chen W, Wong MW, Gonzalez C, Pople JA (2004) Gaussian, Inc., Wallingford
- Baerends AD FEJ, Autschbach J, Bérces A, et al. Amsterdam density functional. Theoretical chemistry, Vrije Universiteit, Amsterdam. <http://www.scm.com>
- Fasman GD (ed) (1996) Circular dichroism and conformational analysis of biomolecules, Springer, New York, p 30ff
- Breest A, Ochmann P, Pulm F, Gödderz H, Carnell M, Hormes J (1994) Mol Phys 82:539. doi:10.1080/00268979400100404
- Neugebauer J, Baerends EJ, Nooijen M, Autschbach J (2005) J Chem Phys 122:234305. doi:10.1063/1.1927519
- Crawford TD, Tam MC, Abrams M (2007) J Chem Phys A 111:12057. doi:10.1021/jp075046u
- Žilinskas A, Stončius S, Butkus EV (2005) Chirality 17:S70. doi:10.1002/chir.20118
- Caldwell DJ, Eyring H (1971) The theory of optical activity. Wiley-Interscience, New York, p 220ff
- Stephens PJ, McCann DM, Butkus E, Stoncius S, Cheeseman JR, Frisch MJ (2004) J Org Chem 69:948. doi:10.1021/jo0357061
- Ho T-L (1995) Symmetry: a basis for synthesis design. Wiley-Interscience, New York
- Gibson SE, Castaldi MP (2006) Chem Comm 3045
- Moberg C (1998) Angew Chem Int Ed 37:248. doi:10.1002/(SICI)1521-3773(19980216)37:3<248::AID-ANIE248>3.0.CO;2-5
- Farina M, Morandi C (1974) Tetrahedron 30:1819. doi:10.1016/S0040-4020(01)97316-8
- Nakazaki M (1984) Top Stereochem 15:199. doi:10.1002/9780470147245.ch3
- Kozhushkov SI, Preuss T, Yufit DS, Howard JAK, Meindl K, Rühl S, Yamamoto C, Okamoto Y, Schreiner PR, Rinderspacher BC, de Meijere A (2006) Eur J Org Chem 2590
- Crawford TD, Owens LS, Tam MC, Schreiner PR, Koch H (2005) J Am Chem Soc 127:1368
- Pedersen TB, Koch HJ (2000) Chem Phys 112:2139
- Mislow K, Glass MAW, O'Brien RE, Rutkin P, Steinberg DH, Weiss J, Djerassi C (1962) J Am Chem Soc 84:1455. doi:10.1021/ja00867a023
- Mislow K, Glass MAW, Hopps HB, Simon E, Wahl GH Jr (1964) J Am Chem Soc 86:1710. doi:10.1021/ja01063a014
- Haas G, Hulbert PB, Klyne W, Prelog V, Sznatzke G (1971) Helv Chim Acta 54:491. doi:10.1002/hlca.19710540208
- Wagniere G (1971) Jerus Symp Quantum Chem Biochem 3:127
- Sagir J, Yogeve A, Mazur Y (1977) J Am Chem Soc 99:6861. doi:10.1021/ja00463a013
- Jackson WM, Mebel AM, Lin SH, Lee YT (1997) J Phys Chem A 101:6338. doi:10.1021/jp970597d